



## Article

# Simultaneous Removal of Arsenate and Fluoride Using Magnesium-Based Adsorbents

Hajime Sugita \* Kazuya Morimoto, Takeshi Saito and Junko Hara

Geological Survey of Japan, National Institute of Advanced Industrial Science and Technology (AIST), Central 7, 1-1-1 Higashi, Tsukuba 305-8567, Japan; kazuya.morimoto@aist.go.jp (K.M.); take-saitou@aist.go.jp (T.S.); j.hara@aist.go.jp (J.H.)

\* Correspondence: hajime.sugita@aist.go.jp

**Abstract:** In this study, arsenate, As(V), and fluoride (F) were simultaneously removed from contaminated water using MgO, Mg(OH)<sub>2</sub>, and MgCO<sub>3</sub> as Mg-based adsorbents, as existing studies only focus on their individual removal. The removal performance of As(V) and F followed the order MgCO<sub>3</sub> < Mg(OH)<sub>2</sub> < MgO. Under the test conditions, MgO and Mg(OH)<sub>2</sub> met the environmental standards for As and F (0.01 and 0.8 mg/L, respectively), but MgCO<sub>3</sub> did not. The As(V) removal performance was not significantly affected by an increase in the initial F concentration. It was concluded that As(V) was adsorbed and removed more preferentially than F by Mg-based adsorbents because a considerable amount of F remained even when the majority of As(V) was removed. Most arsenic (As)-adsorption data for MgO fit the Langmuir and Freundlich models, whereas those for Mg(OH)<sub>2</sub> did not fit either model well. Additionally, the As-adsorption data for MgCO<sub>3</sub> fit the Freundlich model but not the Langmuir model. Most of the F-adsorption data for the Mg-based adsorbents fit the Langmuir and Freundlich models. The removal mechanisms of As(V) and F using Mg-based adsorbents were assumed to be predominantly caused by ion-exchange and chemical-adsorption reactions on the adsorbent surface because no magnesium arsenate, magnesium fluoride, or magnesium hydroxide fluoride species were observed in the X-ray diffraction analysis. This research advances the sustainable As–F simultaneous treatment method using inexpensive adsorbents.



**Citation:** Sugita, H.; Morimoto, K.; Saito, T.; Hara, J. Simultaneous Removal of Arsenate and Fluoride Using Magnesium-Based Adsorbents. *Sustainability* **2024**, *16*, 1774. <https://doi.org/10.3390/su16051774>

Academic Editor: Haradhan Kolya

Received: 27 December 2023

Revised: 15 February 2024

Accepted: 16 February 2024

Published: 21 February 2024



**Copyright:** © 2024 by the authors. Licensee MDPI, Basel, Switzerland. This article is an open access article distributed under the terms and conditions of the Creative Commons Attribution (CC BY) license (<https://creativecommons.org/licenses/by/4.0/>).

## 1. Introduction

Arsenic (As) and fluoride (F) contamination, both anthropogenic and natural, occur worldwide, with high levels of contamination reported in countries such as China, Pakistan, India, Mexico, Argentina, and Chile [1–7]. One of the studies on the anthropogenic co-contamination of As and F was conducted by Farooqi et al. (2008), in which the sources of the contamination were fertilizers, combusted coal, and industrial waste [3]. Alarcón-Herrera et al. (2013) studied the co-contamination of As and F in arid and semi-arid regions of Latin America [5]. According to them, As and F contamination results from water–rock interactions were found, where high As concentrations often show a direct relationship with high F concentrations. The origin of As and F in groundwater in Latin America is mainly geogenic by nature, with the primary source identified as volcanic glass and, to a lesser extent, hydrothermal minerals. Additionally, the secondary source was Fe-, Mn-, and Al-oxides/hydroxides and clays [5]. Furthermore, according to Navarro et al. (2017), most of the large-scale contamination of groundwater is of geological origins, such as the oxidation reaction of sulfide minerals in metasedimentary rocks for As and the water–rock interaction with fluorite (CaF<sub>2</sub>) for F [6].

Toxic substances are often found in industrial effluents, mine effluents, and natural groundwater. Many people in developing regions directly drink contaminated groundwater. The World Health Organization (WHO) guidelines on drinking water quality set a

provisional value of 0.01 mg/L for As and introduced the concept of toxic effects on the human body [8]. In Japan, the environmental and effluent standards for As have been established as 0.01 at 0.1 mg/L, respectively. The prevention of As health hazards can only be achieved by properly treating As-contaminated water. Various methods for purifying As-contaminated water have been researched and developed, such as the coprecipitation method using flocculants; the ion-exchange method using ion-exchange resins; adsorption methods using adsorbents such as activated carbon, silica gel, iron-based adsorbents, and aluminum-based adsorbents; microfiltration methods using microfiltration membranes, nanofiltration membranes, ultrafiltration membranes, and reverse osmosis filtration membranes; chemical or biological oxidation methods; and electrocoagulation methods [9–12]. Despite these various As-removal methods, in developing countries, As treatment methods using inexpensive adsorbents have high potential because of their low cost and easy operation. Among these adsorbents, magnesium (Mg)-based adsorbents are expected to exhibit high As-removal performance.

Yu et al. (2011) investigated the removal of As using MgO- and MgCO<sub>3</sub>-based adsorbents [13]. They created two types of hydromagnesite (MgCO<sub>3</sub>-based adsorbents) using Mg(NO<sub>3</sub>)<sub>2</sub> and K<sub>2</sub>CO<sub>3</sub> as raw materials. Each hydromagnesite was then fired to create two types of MgO-based adsorbents. The specific surface areas of the two types of hydromagnesite were approximately 21 and 18 m<sup>2</sup>/g, respectively, whereas those of the two types of MgO-based adsorbents were approximately 25 and 33 m<sup>2</sup>/g, respectively. They conducted adsorption tests for arsenite As(III) and arsenate As(V) using the adsorbents. MgO-based adsorbents were shown to have a higher adsorption performance for both As(III) and As(V) than hydromagnesites. Therefore, subsequent studies have only focused on MgO-based adsorbents. The adsorption data for MgO-based adsorbents were applied to the Langmuir and Freundlich models. The adsorption data for As(III) fit the Freundlich model better than that of the Langmuir model. The As(III)-adsorption capacities of the two types of MgO-base adsorbents reached approximately 644 and 252 mg/g at equilibrium concentrations of 7.8 and 4.5 mg/L, respectively. The As(V) adsorption data for MgO-based adsorbents fit the Langmuir model better than the Freundlich model. The maximum capacities of these two types of MgO-based adsorbents for As(V) were approximately 344 and 379 mg/g, respectively [13].

Lin et al. (2023) investigated As-removal using Mg(OH)<sub>2</sub>-based adsorbents [14]. They conducted As(V) removal tests using monodispersed porous pinecone-like Mg(OH)<sub>2</sub>, a type of Mg(OH)<sub>2</sub>-based adsorbent. The Mg(OH)<sub>2</sub>-based adsorbent was prepared by dissolving MgSO<sub>4</sub> and mannitol (C<sub>6</sub>H<sub>14</sub>O<sub>6</sub>) in ultrapure water, sonicating, collecting the precipitate under alkaline conditions, and freeze-drying. The adsorbent consisted of monodispersed pinecone-like spheres with a size of approximately 3 μm and a surface area of 63.1 m<sup>2</sup>/g. They reported that after As(V) adsorption, the diffraction peaks of Mg(OH)<sub>2</sub> completely disappeared, and only the characteristic peak of Mg<sub>3</sub>(AsO<sub>4</sub>)<sub>2</sub>·8H<sub>2</sub>O was present. Standard adsorption tests were conducted at an adsorbent concentration of 0.5 g/L. Approximately 38% of As was removed at an initial As concentration of 1254 mg/L, corresponding to 945.8 mg/g at equilibrium. The As-removal ratio at 1.1 mg/L was approximately 100%, corresponding to 2.2 mg/g at equilibrium. The As-removal efficiency decreased under acidic and basic conditions. In the pH range of 3–12, the As-removal efficiency was neutrally symmetric after the adsorption equilibrium. Research on the effects of coexisting anions showed that Cl<sup>−</sup>, NO<sub>3</sub><sup>−</sup>, and SO<sub>4</sub><sup>2−</sup> had little effect on the adsorbent, whereas CO<sub>3</sub><sup>2−</sup> and PO<sub>4</sub><sup>3−</sup> significantly inhibited As(V) removal. However, in adsorption tests using industrial wastewater, the influence of competing ions on adsorption was not significant. Therefore, they concluded that it is an excellent adsorbent that can be applied to industrial wastewater treatment [14].

However, both As and F are eluted from marine sediments, which may lead to the contamination of the surrounding groundwater and soil. Although F is an essential substance for the human body, its excessive intake is known to cause various health hazards, and the WHO has set a guideline value of 1.5 mg/L for drinking water [8]. Japan has an

environmental standard of 0.8 mg/L and effluent standards of 8 mg/L (outside of marine areas) with 15 mg/L (in marine areas) for F. Many studies have reviewed different methods for F-removal, such as coagulation–precipitation, ion-exchange, membrane separation, and adsorption [15–18]. Pillai et al. (2021) also described that membrane and ion-exchange methods are not regularly used in developing countries such as India because of their high cost and maintenance, whereas coagulation–precipitation, and adsorption are predominantly used in India [18]. Aluminum-, carbon-, and natural-based adsorbents, nanoparticles, and other materials have been investigated for use as adsorbents for F-removal [15–18]. In addition, much research has been conducted on Mg-based adsorbents for F-removal.

Jin et al. (2015) investigated the removal of F using MgO-based adsorbents [19]. They created porous MgO nanoplates with a BET (Brunauer–Emmett–Teller)-specific surface area of 47.4 m<sup>2</sup>/g via heating and cooling a mixed aqueous solution of MgCl<sub>2</sub> with urea and calcining the resulting precipitate. Additionally, adsorption tests were conducted using MgO-based adsorbents. They reported that when the F-equilibrium concentration was 114.5 mg/L at a pH of 7.0, the F-adsorption capacity was 185.5 mg/g. Moreover, the F-adsorption behavior was better suited to the Freundlich model than the Langmuir model. In addition, they reported that the F-removal rate hardly changed in the pH range of 2 to 11 but rapidly decreased above a pH of 12. They attributed this to the competition for adsorption sites between hydroxide and F ions. Regarding the influence of coexisting anions, they reported that Cl<sup>−</sup>, SO<sub>4</sub><sup>2−</sup>, and NO<sub>3</sub><sup>−</sup> had little effect on F-adsorption but inhibited F-removal in the order of HCO<sub>3</sub><sup>−</sup> < CO<sub>3</sub><sup>2−</sup> < PO<sub>4</sub><sup>3−</sup>. Furthermore, FTIR (Fourier Transform Infrared Spectroscopy) analysis revealed peaks due to the formation of Mg(OH)<sub>2</sub> via the reaction with water, the binding of MgO molecules on the adsorbent surface to CO<sub>2</sub> molecules in the air, and a new peak that appears to indicate the formation of MgF. Because the carbonate peak was lost in F solutions above 300 mg/L, they concluded that not only surface hydroxyl groups but also surface carbonate can be ion-exchanged with F [19].

Wallace et al. (2019) investigated F-removal using Mg(OH)<sub>2</sub>-based adsorbents [20]. They conducted fluorine adsorptive removal tests on 11 types of nanomaterials, including brucite (a Mg(OH)<sub>2</sub>-based adsorbent), and reported that brucite was an adsorbent with excellent F-removal performance comparable to that of ferrihydrite and apatite. A negative relationship was found between the F-adsorption capacity and the specific surface area of the selected nanomaterials. The specific surface area of brucite was reported to be 104.9 m<sup>2</sup>/g, whereas the F-adsorption capacity at an adsorption equilibrium time of 48 h was 0.59 mg/g, and the F-adsorption capacity relative to the specific surface area was 0.037 mg/m<sup>2</sup>. They concluded from batch test results that the F-adsorption behavior fit the Freundlich and Redlich–Peterson models better than the Langmuir model. Desorption tests were also performed during the column tests; however, the F-desorption efficiency (4–9%) was low, suggesting the difficulty in reusing the adsorbent [20].

Investigations on the simultaneous removal of As and F have also attracted attention in recent years. Ingallinella et al. (2011) conducted laboratory and pilot scale studies using natural water with As concentrations from 60 to 90 µg/L and F concentrations ranging from 2.4 to 3.2 mg/L [4]. They used polyaluminum chloride (PACl) as a flocculant and, in addition, initially also used sulfuric acid for pH adjustment. After the process, sodium hydroxide was added to reduce residual aluminum in the treated water below a limit value (0.20 mg/L). They reported that their optimized process achieved removal efficiencies of 75–85% for As and 50–55% for F [4]. López-Guzmán et al. (2019) performed the simultaneous removal of As and F from well water using an electrocoagulation process with iron and aluminum electrodes [21]. Although F was removed due to aluminum species generated in the aluminum electrode, the F-removal efficiency decreased in the presence of As because As competed with F for the adsorption sites of the formed aluminum hydroxide, while the high removal efficiency of As was obtained without being affected by F, probably because As was removed due to the coagulant species generated in the iron electrode. They reported that the optimum conditions for their process were a current density of 4.5 mA/cm<sup>2</sup>, an initial pH of 5, and a treatment time of 15 min, when initial concentrations

of As and F were 0.08 mg/L and 5 mg/L, respectively, and under these conditions, the removal ratios of As and F were achieved at approximately 100% and 86%, respectively [21]. Tolkou et al. (2023) investigated the removal of As(III) and F using manganese oxides supported on graphene nanostructures (GO-MnO<sub>2</sub>) [22]. According to the results, the fluoride removal efficiency increased with increasing arsenic concentrations, and arsenic removal increased with increasing fluoride concentrations, mainly at a neutral pH value. Subsequently, the adsorption behavior of As(III) and F was evaluated using adsorption isotherms. They reported that the Langmuir isotherm model better fit the adsorption of As(III) in the presence of F-, and the Freundlich isotherm model better fit the adsorption of F- in the presence of As(III). Furthermore, their study confirmed the reuse of the GO-MnO<sub>2</sub> adsorbent for four cycles of As(III) removal and three cycles for F ions after regeneration treatment using NaOH [22].

As mentioned above, many studies have been conducted on the removal of As and F using Mg-based adsorbents; however, little research has been conducted on the simultaneous removal of As and F. Therefore, the purpose of this study was to obtain basic information on the simultaneous removal of As(V)-F using various types of Mg compounds as Mg-based adsorbents. Simultaneous As(V)-F-removal tests were performed using multiple synthetic contaminated waters in which As(V) and F coexist using three types of Mg-based adsorbents (MgO, Mg(OH)<sub>2</sub>, and MgCO<sub>3</sub>). Based on the results obtained from the removal tests, we report the As(V)- and F-removal performance of each Mg-based adsorbent and the analytical results of the As(V)- and F-adsorption behavior using adsorption isotherms.

## 2. Materials and Methods

The reagents listed in this article were purchased from FUJIFILM Wako Pure Chemical Corporation (formerly Wako Pure Chemical Industries, Ltd., Osaka, Japan) unless specified otherwise.

### 2.1. Mg-Based Adsorbents

Commercial powder reagents of MgO, Mg(OH)<sub>2</sub>, and MgCO<sub>3</sub> (FUJIFILM Wako Chemical Co.) were used as Mg-based adsorbents. The measured Mg content  $\alpha_{\text{Mg}}$  (%), reagent purity (obtained from  $\alpha_{\text{Mg}}$  and  $\alpha_{\text{Ca}}$ ) P (%), median particle size  $D_{\text{p}50}$  ( $\mu\text{m}$ ), and BET surface area  $S_{\text{BET}}$  ( $\text{m}^2/\text{g}$ ) are listed in Table 1. The data in Table 1 were obtained from a previous study [23]. The primary reason for P not equaling 100% was the adsorbed water.

**Table 1.** Characteristics of the adsorbents where  $\alpha$  is the measured Mg content, P is the reagent purity,  $D_{\text{p}50}$  is the median particle size, and  $S_{\text{BET}}$  is the BET surface area.

No.	Adsorbent	$\alpha_{\text{Mg}}$ (%)	P (%)	$D_{\text{p}50}$ ( $\mu\text{m}$ )	$S_{\text{BET}}$ ( $\text{m}^2/\text{g}$ )
(1) <sup>1</sup>	MgO	59.1	98.0	1.54	4.3
(2) <sup>1</sup>	Mg(OH) <sub>2</sub>	40.6	97.3	4.13	22.0
(3) <sup>1</sup>	MgCO <sub>3</sub>	24.8	86.1	15.0	26.0

<sup>1</sup> Data from Sugita et al. (2016) [23].

### 2.2. Synthetic As(V)-F in Multi-Contaminated Water

An aqueous solution of As(V) was prepared by dissolving the Na<sub>2</sub>HAsO<sub>4</sub>·7H<sub>2</sub>O powder reagent in ion-exchanged water. Synthetic As(V)-F-contaminated water was prepared by mixing and diluting the As(V) aqueous solution, a sodium fluoride aqueous solution (F standard solution for ion chromatography analysis), and ion-exchange water at a predetermined ratio. The pH was adjusted to approximately 7 using aqueous HNO<sub>3</sub> and NaOH. The initial As concentration  $C_{\text{AS}0}$  was 1 mg/L, and the initial F concentration  $C_{\text{F}0}$  was 15, 30, or 60 mg/L in synthetic As(V)-F-contaminated water. The pH and ORP, immediately after pH adjustments, are referred to as the initial pH ( $pH_0$ ) and initial ORP ( $ORP_0$ ), respectively.

### 2.3. As–F Simultaneous Removal Tests

A given amount of the adsorbent was placed in a TPX (polymethylpentene) beaker, and 100 mL of synthetic-contaminated water was added. The maximum adsorbent addition concentration  $W_{Ad0}/V$  (where  $W_{Ad0}$  is the amount of adsorbent added, and  $V$  is the liquid volume [L]) in this study was 1–5 g/L for MgO (depending on  $C_{F0}$ ) and 60 g/L for Mg(OH)<sub>2</sub> and MgCO<sub>3</sub>. The solution was stirred for 24 h. The solution was then centrifuged, filtered (0.45 µm), and stored in a polypropylene bottle. The pH and ORP of the filtered solution were measured using pH and ORP meters (LAQUA F-72, HORIBA, Ltd., Kyoto, Japan), respectively. The As, Mg, and F in the solutions were analyzed using inductively coupled plasma–mass spectrometry (Agilent 7700X, Agilent Technologies, Inc., Hachioji, Japan), inductively coupled plasma–atomic emission spectrometry (SII SPS3500DD, Thermo Fisher Scientific K.K., Tokyo, Japan), and ion chromatography (Thermo Scientific Dionex Integron RFIC, Seiko Instruments Inc., Chiba, Japan).

The reasons for the difference in  $W_{Ad0}/V$  between MgO and the other two adsorbents in the removal test are as follows: preliminary tests showed that the MgO adsorbent has a higher As-removal performance than the other two adsorbents and can remove almost 100% of As(V) even at a fairly low  $W_{Ad0}/V$ . One of the objectives of this study is to confirm whether fluoride affects the As-removal performance of Mg-based adsorbents. To facilitate this confirmation, in this study, the  $W_{Ad0}/V$  for MgO was set to a lower concentration range than that for the other two adsorbents.

### 2.4. Preparation of Samples for X-ray Diffraction (XRD) Analysis

To examine the forms of As(V) and F adsorbed with Mg-based adsorbents, MgO, Mg(OH)<sub>2</sub>, and MgCO<sub>3</sub> were adsorbed with As(V) and F, respectively. Synthetic As(V)-contaminated water with a  $C_{AS0}$  value of 10 mg/L was used to prepare As-adsorbed Mg-based adsorbents. Synthetic F-contaminated water with  $C_{F0} = 60$  mg/L was used to prepare F-adsorbed Mg-based adsorbents. Thereafter, Mg-based adsorbents were added to  $W_{Ad0}/V = 2$  g/L of each synthetic contaminated water sample. After stirring for 24 h, the solution was subjected to suction filtration. The collected, filtrated adsorbent was then dried overnight at 40 °C. The constituent phases of the prepared samples were identified using a powder XRD (RINT-2500, Rigaku Co., Akishima, Japan) at GSJ-Lab, AIST.

## 3. Results

### 3.1. Residual as Concentration in Treated Water

The residual As concentration in the treated water,  $C_{AS}$  [mg/L], obtained from the removal tests is shown in Figure 1. Figure 1a–c show MgO, Mg(OH)<sub>2</sub>, and MgCO<sub>3</sub>, respectively.

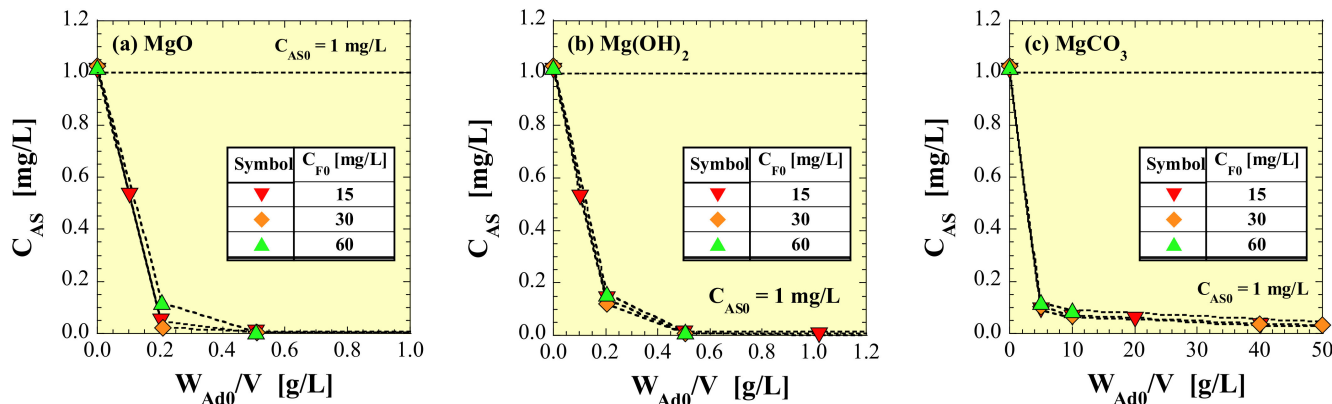


**Figure 1.** Change in residual As concentration in treated water with adsorbent addition concentration: (a) MgO, (b) Mg(OH)<sub>2</sub>, and (c) MgCO<sub>3</sub>.

These figures show that  $C_{AS}$  decreased with increasing  $W_{Ad0}/V$ , regardless of the type of adsorbent or  $C_{F0}$ . In addition, for all the Mg-based adsorbents,  $C_{AS}$  tended to increase slightly with increasing  $C_{F0}$ , but the influence of  $C_{F0}$  on  $C_{AS}$  was extremely small. For the same  $W_{Ad0}/V$ , the  $C_{AS}$  values followed the order  $MgO < Mg(OH)_2 < MgCO_3$ . In other words, the As-removal performance followed the order  $MgCO_3 < Mg(OH)_2 < MgO$ . In addition,  $MgO$  and  $Mg(OH)_2$  met the environmental standards for As ( $0.01\text{ mg/L}$ ) by increasing  $W_{Ad0}/V$ . Although  $MgCO_3$  could meet the effluent standard of As ( $0.1\text{ mg/L}$ ), it could not meet the environmental standard, even at the highest  $W_{Ad0}/V = 60\text{ g/L}$  test conditions used in this study.

### 3.2. Residual F Concentration in Treated Water

The residual F concentration in the treated water,  $C_F$  [ $\text{mg/L}$ ], obtained from the removal tests is shown in Figure 2. Similar to Figure 1, Figure 2a–c show  $MgO$ ,  $Mg(OH)_2$ , and  $MgCO_3$ , respectively.

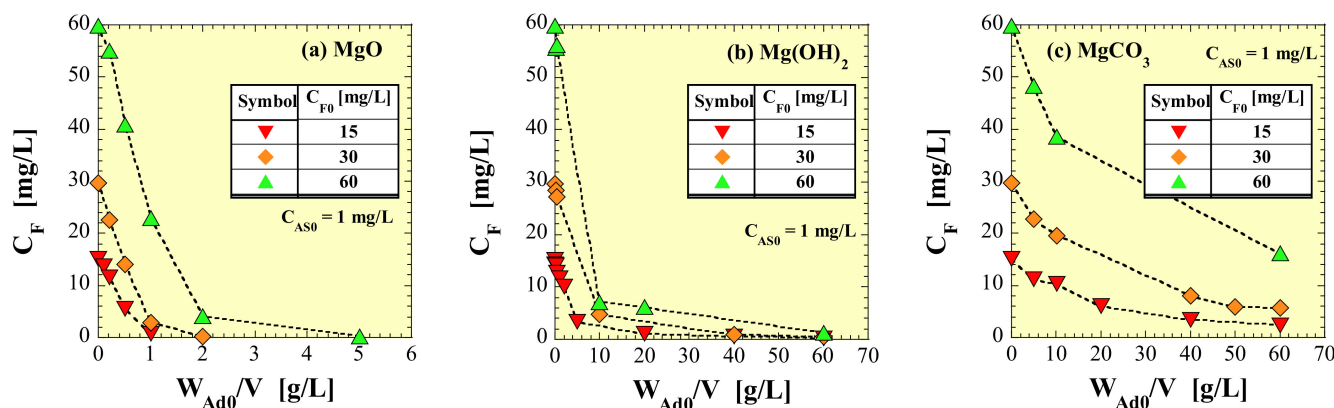


**Figure 2.** Plots of residual F concentration in treated water versus adsorbent addition concentration: (a)  $MgO$ , (b)  $Mg(OH)_2$ , and (c)  $MgCO_3$ .

Similar to  $C_{AS}$ , regardless of the type of adsorbent and the value of  $C_{F0}$ ,  $C_F$  decreased with increasing  $W_{Ad0}/V$ . The  $C_F$  values for the same  $C_{F0}$  and  $W_{Ad0}/V$  were in the order  $MgO < Mg(OH)_2 < MgCO_3$ . In other words, the F-removal performance followed the order  $MgCO_3 < Mg(OH)_2 < MgO$ . This superiority order is the same as that for the As-removal performance. In addition,  $MgO$  could meet the environmental standard of F ( $0.8\text{ mg/L}$ ) regardless of  $C_{F0}$ . Except for  $C_{F0} = 60\text{ mg/L}$ ,  $Mg(OH)_2$  met the environmental standard for F under the test conditions, and even  $C_{F0} = 60\text{ mg/L}$  met the effluent standard for F in areas other than the marine areas ( $8\text{ mg/L}$ ). By contrast,  $MgCO_3$  only met effluent standard F at  $C_{F0} = 15$  and  $30\text{ mg/L}$  under the test conditions.

In addition, a comparison of Figures 1 and 2 shows that for all three types of Mg-based adsorbents, regardless of  $C_{F0}$ , the  $C_F$  is much higher than zero, even at  $W_{Ad0}/V$ , where the  $C_{AS}$  is close to zero. Thus, it can be concluded that the Mg-based adsorbents adsorbed and removed As(V) preferentially rather than F.

### 3.3. Leached Mg Concentration in Treated Water

Naturally, the base material of a Mg-based adsorbent (such as the Mg component) leaches into the aqueous solution. The leached Mg concentration in the treated water,  $C_{Mg}$  [ $\text{mg/L}$ ], obtained from the removal tests, is shown in Figure 3. Figure 3a–c show  $MgO$ ,  $Mg(OH)_2$ , and  $MgCO_3$ , respectively.

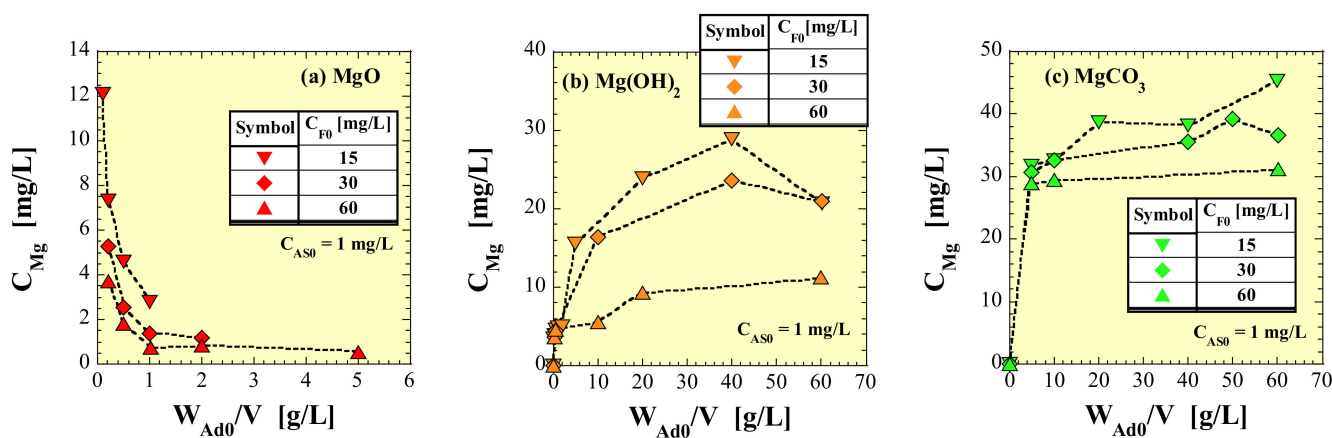


**Figure 3.** Plots of leached Mg concentration in treated water versus adsorbent addition concentration: (a) MgO, (b) Mg(OH)<sub>2</sub>, and (c) MgCO<sub>3</sub>.

Regardless of the type of adsorbent, there was an overall tendency for the  $C_{Mg}$  to decrease with increasing  $C_{F0}$ . However, unlike the behavior of  $C_{AS}$  and  $C_F$ , the behavior of  $C_{Mg}$  toward  $W_{Ad0}/V$  varied significantly depending on the type of adsorbent. The  $C_{Mg}$  for MgO decreases with increasing  $W_{Ad0}/V$  (Figure 3a). The  $C_{Mg}$  for Mg(OH)<sub>2</sub> tends to increase and then decrease with increasing  $W_{Ad0}/V$  ( $C_{F0} = 15$  and 30 mg/L in Figure 3b). The behavior of  $C_{Mg}$  for MgCO<sub>3</sub> appeared to differ depending on  $C_{F0}$ ; however, overall,  $C_{Mg}$  seemed to gradually increase alongside the trend of increasing  $W_{Ad0}/V$  (Figure 3c).

### 3.4. pH of Treated Water

The pH of the treated water (final pH),  $pH_f$ , obtained from the removal tests is shown in Figure 4. Figure 4a–c show MgO, Mg(OH)<sub>2</sub>, and MgCO<sub>3</sub>, respectively.

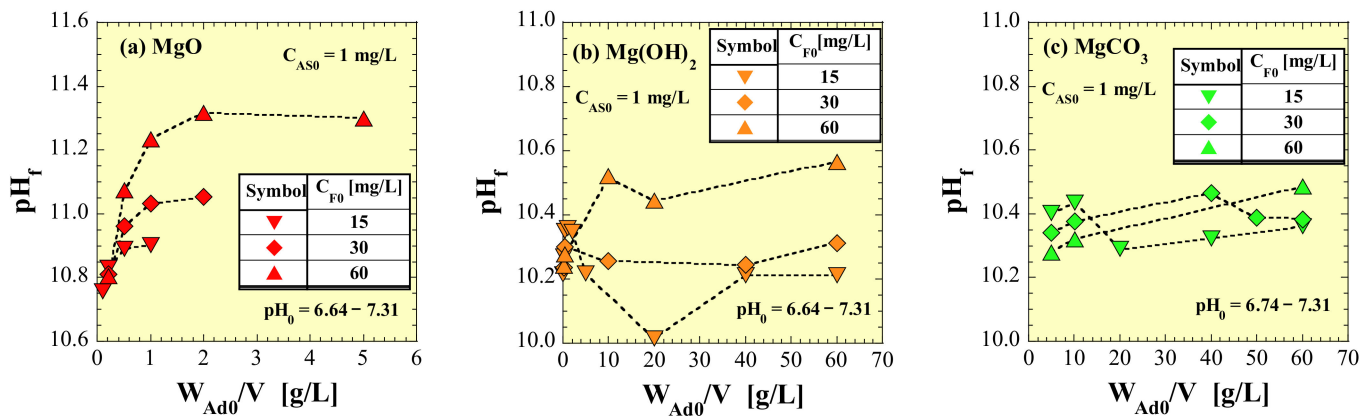


**Figure 4.** Plots of the pH of treated water versus adsorbent addition concentration: (a) MgO, (b) Mg(OH)<sub>2</sub>, and (c) MgCO<sub>3</sub>.

The  $pH_f$  for MgO increased with increasing  $W_{Ad0}/V$  and then remained almost constant;  $pH_f$  clearly increased as  $C_{F0}$  increased (Figure 4a). The effects of  $W_{Ad0}/V$  on  $pH_f$  for Mg(OH)<sub>2</sub> are not clear, but as with MgO,  $pH_f$  appeared to increase as  $C_{F0}$  increased (Figure 4b). However, the  $pH_f$  of MgCO<sub>3</sub> was not clearly affected by the difference in  $W_{Ad0}/V$  or in  $C_{F0}$  (Figure 4c).

### 3.5. ORP of Treated Water

The ORP of the treated water (final ORP),  $ORP_f$ , obtained from the removal tests is shown in Figure 5. Figure 5a–c show MgO, Mg(OH)<sub>2</sub>, and MgCO<sub>3</sub>, respectively.

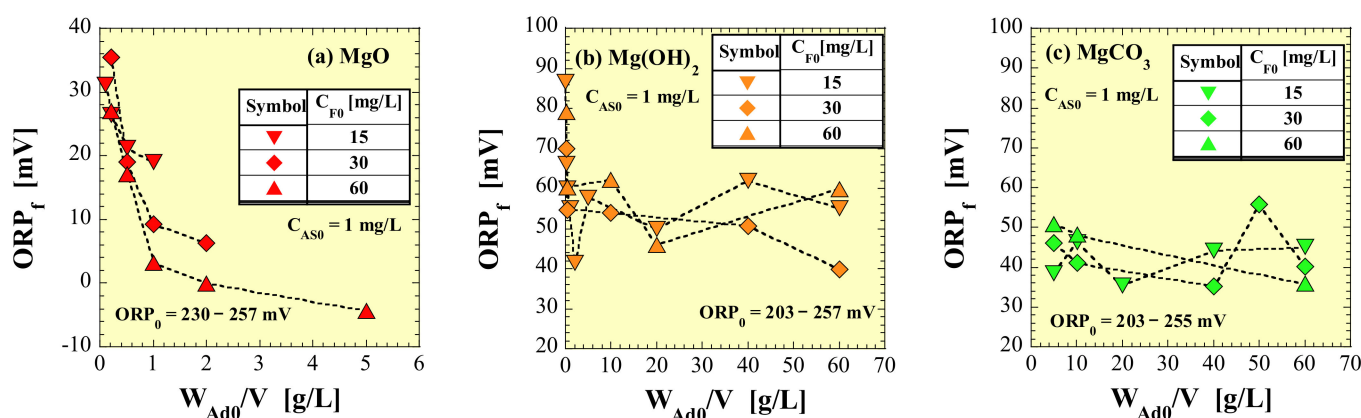


**Figure 5.** Plots of ORP of treated water versus adsorbent addition concentration: (a) MgO, (b) Mg(OH)<sub>2</sub>, and (c) MgCO<sub>3</sub>.

Contrary to the behavior of  $pH_f$ , the  $ORP_f$  for MgO decreased with increasing  $W_{Ad0}/V$ . In addition, there was a tendency that the higher the  $ORP_f$ , the lower the  $C_{F0}$ . Although the  $ORP_f$  for MgO did not reach constant values in the test ranges,  $ORP_f$  might reach constant values if  $W_{Ad0}/V$  increases further. The  $ORP_f$  for Mg(OH)<sub>2</sub> took relatively high values when  $W_{Ad0}/V$  was extremely small (approximately 0.2 g/L) and then decreased when  $W_{Ad0}/V$  was increased slightly. No clear trend was observed in the behavior of  $ORP_f$  with further increased in  $W_{Ad0}/V$  (Figure 5b). The  $ORP_f$  for MgCO<sub>3</sub>, similar to  $pH_f$ , was not clearly affected by the difference in  $W_{Ad0}/V$  or  $C_{F0}$  (Figure 5c).

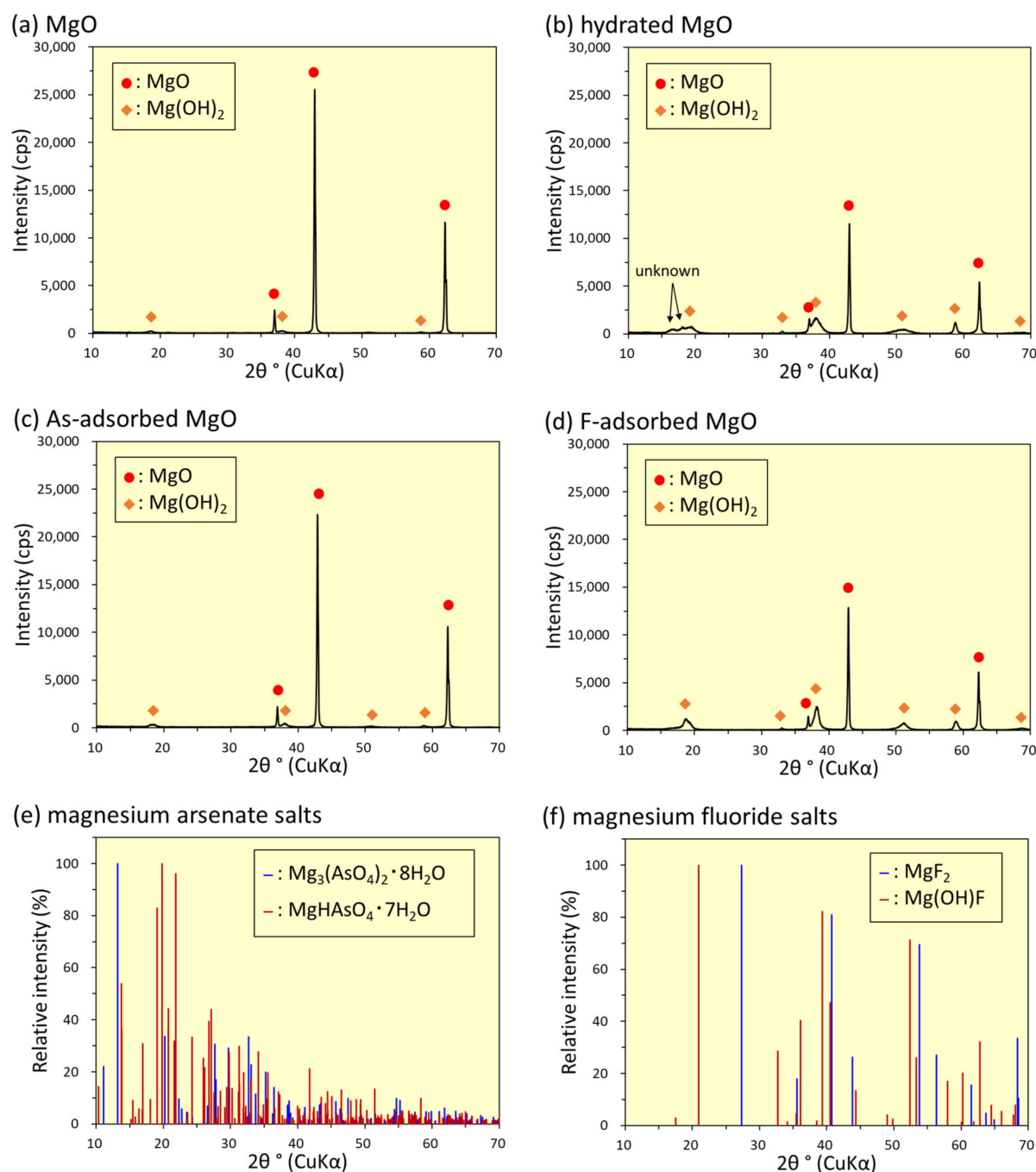
### 3.6. XRD Analysis

The results of the powder XRD analysis for MgO, Mg(OH)<sub>2</sub>, and MgCO<sub>3</sub> are shown in Figures 6, 7, and 8, respectively.

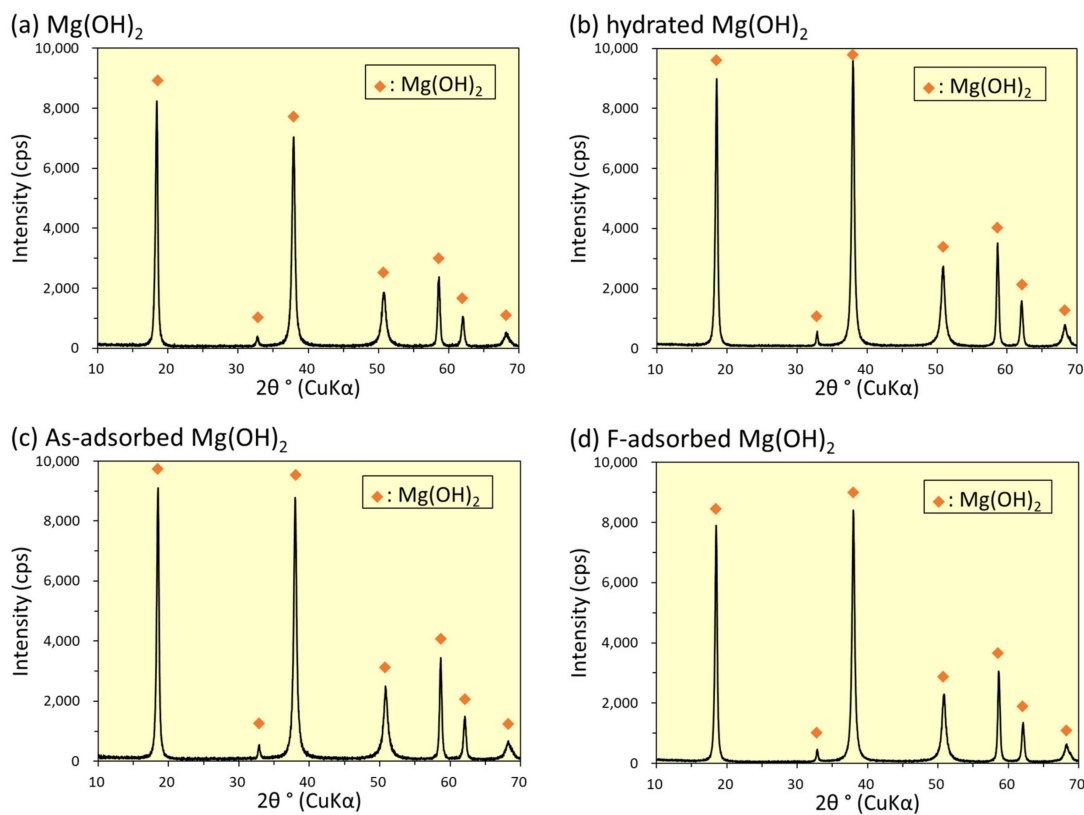
Figure 6a–d show the XRD patterns of unused, hydrated, As-adsorbed, and F-adsorbed MgO, respectively. Figure 6a shows the presence of mostly MgO and trace amounts of Mg(OH)<sub>2</sub> in unused MgO. However, the distinct peaks attributed to Mg(OH)<sub>2</sub> can be seen along with the peaks of MgO in the hydrated MgO sample (Figure 6b), indicating that Mg(OH)<sub>2</sub> was formed via the hydration reaction of MgO. Broad peaks (indicated as unknown in Figure 6b) were observed at a lower angle than the peak around  $2\theta = 18.6^\circ$ , which is attributed to the basal spacing of Mg(OH)<sub>2</sub>. The diffraction pattern of the As-adsorbed MgO (Figure 6c) showed peaks of MgO and Mg(OH)<sub>2</sub>, but the formation of Mg(OH)<sub>2</sub> was clearly less than that of hydrated MgO (Figure 6b). No diffraction peaks attributed to the magnesium arsenate species (such as Mg<sub>3</sub>(AsO<sub>4</sub>)<sub>2</sub> and MgHAsO<sub>4</sub>) were observed in Figure 6c, as can be seen from the comparison with the XRD profiles of Mg<sub>3</sub>(AsO<sub>4</sub>)<sub>2</sub>·8H<sub>2</sub>O (hornesite) derived from Rojo et al. (1996) [24] and MgHAsO<sub>4</sub>·7H<sub>2</sub>O (rosslerite) derived from Ferraris and Franchini-Angela (1973) [25] shown in Figure 6e. Peaks attributed to MgO and Mg(OH)<sub>2</sub> are also observed in Figure 6d, suggesting that Mg(OH)<sub>2</sub> formation is comparable to that of hydrated MgO (Figure 6b). No diffraction peaks of the co-precipitated salts (such as MgF<sub>2</sub> and Mg(OH)F) were also observed in Figure 6d, as evidenced by comparison with the diffraction data of MgF<sub>2</sub> (sellaita) from Baur and Khan (1971) [26] and Mg(OH)F from Crichton et al. (2012) [27] shown in Figure 6f.

Figure 7a shows the XRD pattern of the unused Mg(OH)<sub>2</sub> adsorbent. The diffraction pattern obtained corresponded to the crystal structure of Mg(OH)<sub>2</sub> (brucite). Figure 8a shows the XRD pattern of the unused MgCO<sub>3</sub> adsorbent, and it was a diffraction pattern attributed to the crystalline structure of Mg<sub>5</sub>(CO<sub>3</sub>)<sub>4</sub>(OH)<sub>2</sub>·4H<sub>2</sub>O (hydromagnesite).

As in the case of the MgO adsorbent mentioned above, the XRD analysis results for the Mg(OH)<sub>2</sub> (Figure 7) and MgCO<sub>3</sub> adsorbents (Figure 8) after adsorption showed no evidence of the formation of magnesium arsenate and magnesium fluoride salts. Therefore, it was concluded that the decreases in As(V) and F in the liquid were due to their adsorption onto the adsorbent.



**Figure 6.** Powder X-ray diffraction patterns: (a) MgO, (b) hydrated MgO, (c) As-adsorbed MgO, and (d) F-adsorbed MgO. Relative intensity ratio of XRD peaks based on the crystal structure: (e) magnesium arsenate salts,  $Mg_3(AsO_4)_2 \cdot 8H_2O$  (hernesite) [24] and  $MgHAsO_4 \cdot 7H_2O$  (rosslerite) [25], (f) magnesium fluoride salts,  $MgF_2$  (sellaite) [26] and  $Mg(OH)F$  [27].



**Figure 7.** Powder X-ray diffraction patterns: (a)  $\text{Mg}(\text{OH})_2$ , (b) hydrated  $\text{Mg}(\text{OH})_2$ , (c) As-adsorbed  $\text{Mg}(\text{OH})_2$ , and (d) F-adsorbed  $\text{Mg}(\text{OH})_2$ .

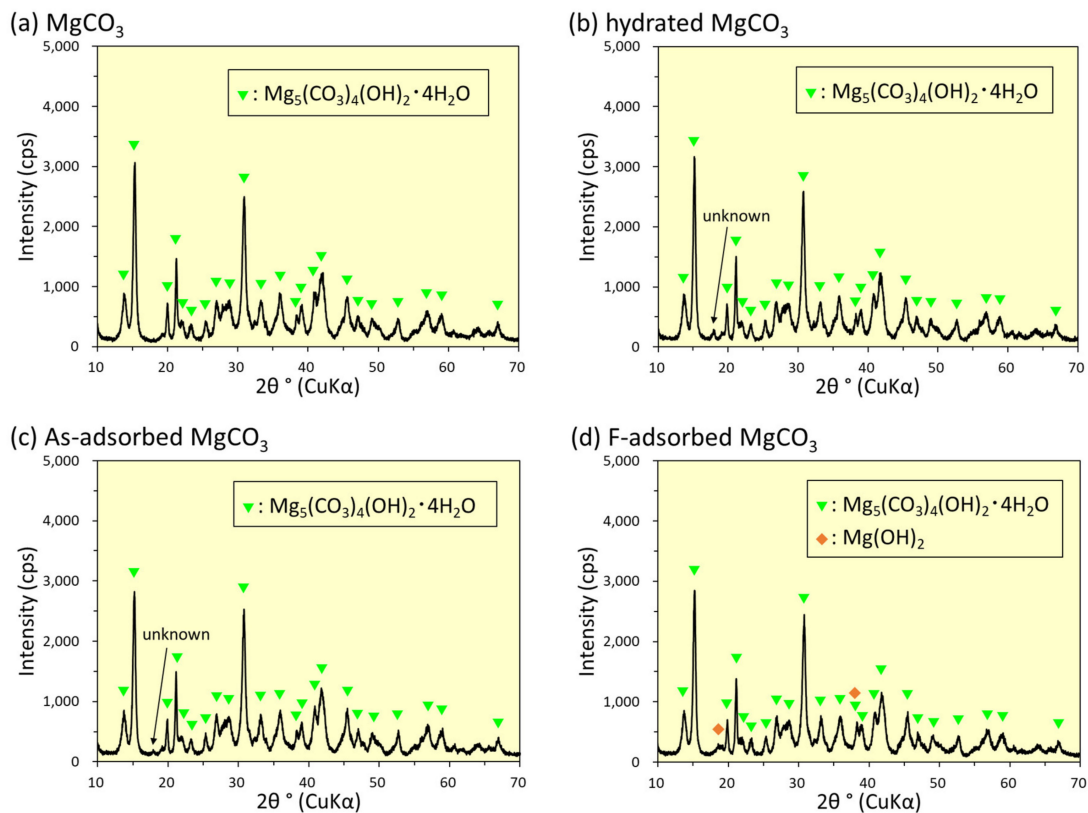


**Figure 8.** Powder X-ray diffraction patterns: (a)  $\text{MgCO}_3$ , (b) hydrated  $\text{MgCO}_3$ , (c) As-adsorbed  $\text{MgCO}_3$ , and (d) F-adsorbed  $\text{MgCO}_3$ .

## 4. Discussion

### 4.1. As-Removal Ratio

The As-removal ratio,  $R_{AS}$  [%], was calculated as follows:

$$R_{AS} = (C_{AS0} - C_{AS})/C_{AS0} \times 100. \quad (1)$$

The  $R_{AS}$  obtained from Equation (1) is plotted versus  $W_{Ad0}/V$  in Figure 9. Figure 9a–c show  $C_{F0}$  values of 15, 30, and 60 mg/L, respectively.

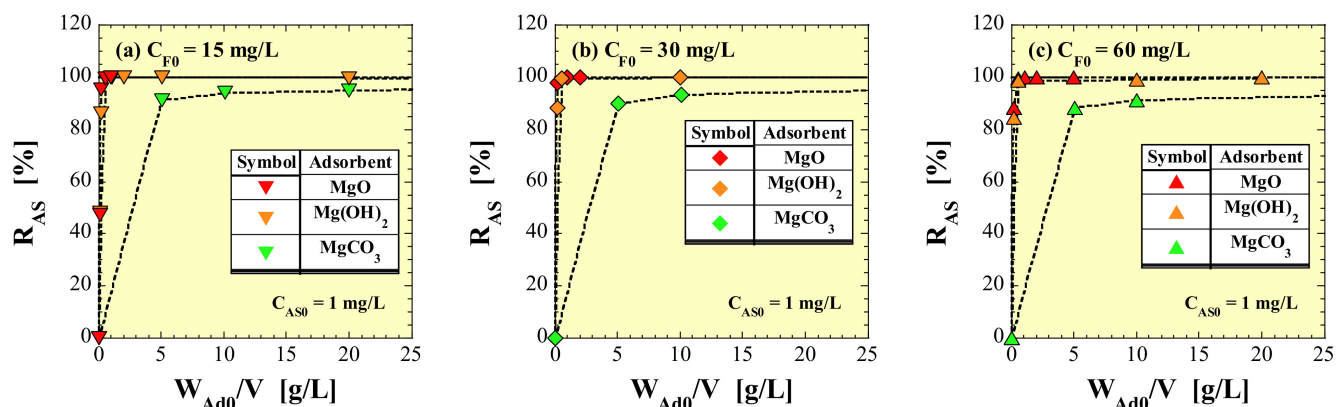


**Figure 9.** Plots of As-removal ratio versus adsorbent addition concentration: (a)  $C_{F0} = 15$  mg/L, (b)  $C_{F0} = 30$  mg/L, and (c)  $C_{F0} = 60$  mg/L.

Comparing the  $R_{AS}$  at the same  $W_{Ad0}/V$  in Figure 9, the As-removal performance of  $MgCO_3$  was the lowest, and those of  $MgO$  and  $Mg(OH)_2$  were almost the same; however,  $MgO$  was slightly better, regardless of  $C_{F0}$ .

Although the As valence differs from this study, Tolkou et al. (2023), who conducted a study on the simultaneous removal of As(III) and F, reported that  $R_{AS}$  increased with increasing  $C_{F0}$ , for example, when  $C_{AS0} = 0.1$  mg/L,  $W_{Ad0}/V = 2$  g/L and  $pH_0 = 7$ ,  $R_{AS} = 84$  and 98% at  $C_{F0} = 0$  and 100 mg/L, respectively [22]. However, in this study, no significant increase in  $R_{AS}$  was observed with increasing  $C_{F0}$ .

Lin et al. (2023) studied As(V)-removal using their synthesized monodisperse porous pinecone-like  $Mg(OH)_2$  (PLMH) [14]. They conducted experiments at various  $C_{AS0}$  (1.1 to 1254 mg/L) and observed the change in  $R_{AS}$  (“Remove Efficiency” in their paper) over time. The  $W_{Ad0}/V$  in their normal tests was 0.5 g/L. Although the equilibrium time varied depending on  $C_{AS0}$ , their test with  $C_{AS0} = 1.1$  mg/L, which was similar to our test conditions, showed that  $R_{AS}$  reached approximately 100% within 10 min. Considering the results of their studies mentioned above, it is considered that the adsorption was sufficiently in equilibrium because the reaction time in this study was 24 h.

### 4.2. F-Removal Ratio

The F-removal ratio,  $R_F$  [%], was calculated as follows:

$$R_F = (C_{F0} - C_F)/C_{F0} \times 100. \quad (2)$$

The  $R_F$  obtained from Equation (2) is plotted versus  $W_{Ad0}/V$  in Figure 10. Figure 10a–c show  $C_{F0}$  values of 15, 30, and 60 mg/L, respectively.

Comparing the  $R_F$  at the same  $W_{Ad0}/V$  in Figure 10, the superiority of the F-removal performance was clearly determined to be  $MgCO_3 < Mg(OH)_2 < MgO$ , regardless of  $C_{F0}$ .

Tolkou et al. (2023) also reported that  $R_F$  increased with increasing  $C_{AS0}$ :  $C_{F0} = 10$  mg/L,  $W_{Ad0}/V = 2$  g/L and  $pH_0 = 7$ ,  $R_F = 74.7$  and 94.3% at  $C_{AS0} = 0$  and 0.5 mg/L, respectively [22]. However, in this study, no significant increase in  $R_{AS}$  was observed with increasing  $C_{F0}$ . However, in this study, it was not possible to evaluate the effects of  $C_{AS0}$  on  $R_F$  because no

tests varying  $C_{AS0}$  as a parameter were conducted. In the future, tests varying  $C_{AS0}$  should be added.

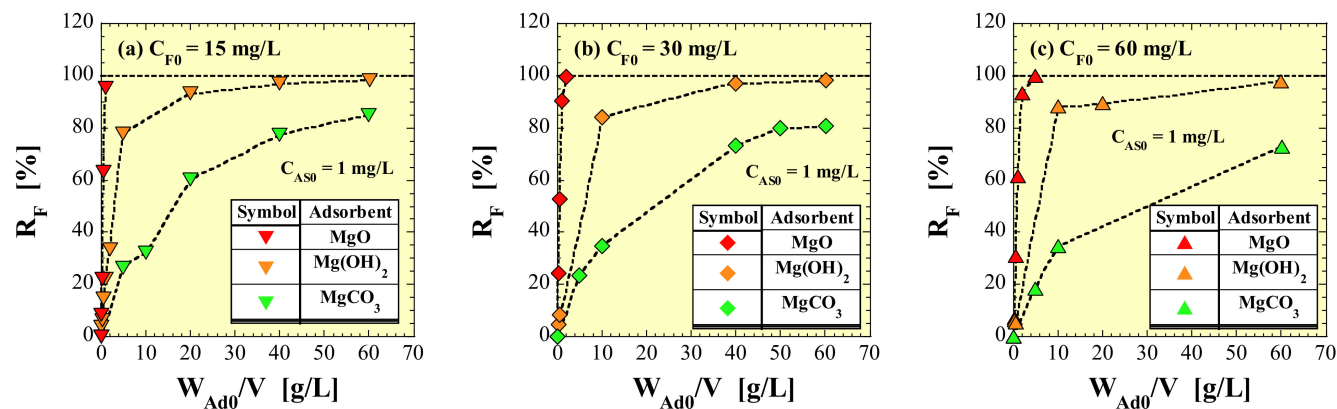
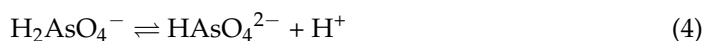


**Figure 10.** Plots of F-removal ratio versus adsorbent addition concentration: (a)  $C_{F0} = 15 \text{ mg/L}$ , (b)  $C_{F0} = 30 \text{ mg/L}$ , and (c)  $C_{F0} = 60 \text{ mg/L}$ .

In this study, the adsorption of both As and F was expected to be close to an equilibrium state because the reaction time was 24 h, as mentioned in Section 4.1. Therefore, the results of this study cannot determine whether both As(V) and F were adsorbed simultaneously or whether the adsorption of one starts after the adsorption of the other is completed. However, because the adsorption amount of As(V) did not change even if the initial concentration of F changed significantly (Figures 1 and 9), it was inferred that F had no significant effect on the adsorption behavior of As(V).

#### 4.3. Dissolved Forms of As(V) and F in Water

The dissolved forms of As(V) in water are represented by the following dissociation reactions for arsenic acid:



where  $pK_{a1} = 2.24$ ,  $pK_{a2} = 6.96$ , and  $pK_{a3} = 11.5$  ( $25^\circ\text{C}$ ) [28], and the abundance of each dissolved arsenic acid species is determined by the following:

$$[\text{H}_2\text{AsO}_4^-]/[\text{H}_3\text{AsO}_4] = 10^{\exp(pH - pK_{a1})} \quad (6)$$

$$[\text{HAsO}_4^{2-}]/[\text{H}_2\text{AsO}_4^-] = 10^{\exp(pH - pK_{a2})} \quad (7)$$

$$[\text{AsO}_4^{3-}]/[\text{HAsO}_4^{2-}] = 10^{\exp(pH - pK_{a3})} \quad (8)$$

For the synthetic contaminated water before adding the adsorbent in this study, the abundances of  $\text{H}_3\text{AsO}_4$  and  $\text{AsO}_4^{3-}$  were considered to be extremely small and negligible because  $pK_{a1} \ll pH_0 \ll pK_{a3}$ . Then, substituting the  $pH_0$  values (6.50–6.62), the values of  $[\text{HAsO}_4^{2-}]/[\text{H}_2\text{AsO}_4^-]$  were calculated to be 0.30–0.46. Therefore, the main dissolved forms of As(V) in synthetic contaminated water were estimated to be  $\text{H}_2\text{AsO}_4^-$  and  $\text{HAsO}_4^{2-}$ , while for the treated water, the abundances of  $\text{H}_3\text{AsO}_4$  and  $\text{H}_2\text{AsO}_4^-$  were considered to be extremely small and negligible because  $pK_{a2} \ll pH_f$ . Then, substituting the  $pH_f$ , the values of  $[\text{AsO}_4^{3-}]/[\text{HAsO}_4^{2-}]$  were calculated to be 0.18–0.65 for MgO, 0.05–0.12 for  $\text{Mg(OH)}_2$ , and 0.06–0.10 for  $\text{MgCO}_3$ . Therefore, the main dissolved forms of As(V) in the treated water were estimated to be  $\text{HAsO}_4^{2-}$  for  $\text{Mg(OH)}_2$  and  $\text{MgCO}_3$ , and  $\text{HAsO}_4^{2-}$  and  $\text{AsO}_4^{3-}$  for MgO.

The dissolved forms of F in water are represented by the following dissociation reactions for hydrofluoric acid:



where  $pK_a = 2.67$  (25 °C) [28], and the abundance of each dissolved hydrofluoric acid species is determined by the following:

$$[\text{F}^-]/[\text{HF}] = 10 \exp(pH - pK_a) \quad (10)$$

From the results obtained by substituting the values of  $pH_0$  (6.43–6.62) and  $pH_f$  (10.0–11.3) into Equation (10), the dissolved form of hydrofluoric acid species in both synthetic contaminated water before adding the adsorbent and treated water was estimated to be approximately 100%  $\text{F}^-$ .

#### 4.4. As- and F-Adsorption Amounts per Unit Mass of Adsorbent

To evaluate the As- and F-adsorption data using general adsorption models, it was necessary to calculate the adsorption amount per unit mass of adsorbent  $Q_{\text{AS}}$  and the F-adsorption amount per unit mass of adsorbent  $Q_F$ . However, to determine  $Q_{\text{AS}}$  and  $Q_F$ , it was necessary to recalculate the concentration of the adsorbent remaining in the solid phase because parts of the base materials of Mg-based adsorbents leached into the aqueous solution, as described in Section 3.3. For this purpose, it was first necessary to determine the adsorbent residual ratio  $\gamma$  [%]. The following describes the calculation of  $\gamma$ ,  $Q_{\text{AS}}$ , and  $Q_F$ .

The initially added Mg amount,  $W_{\text{Mg}0}$  [g], is determined using  $\alpha_{\text{Mg}}$ , as shown in Table 1:

$$W_{\text{Mg}0} = (\alpha_{\text{Mg}}/100) W_{\text{Ad}0}. \quad (11)$$

Next, the amount of Mg remaining as a solid phase,  $W_{\text{Mgf}}$  [g], 24 h after adding the adsorbent is calculated.

$$W_{\text{Mgf}} = W_{\text{Mg}0} - (C_{\text{Mg}}/1000) V. \quad (12)$$

Because the unit of  $C_{\text{Mg}}$  is [mg/L], it is divided by 1000 to convert the unit to [g]. Assuming that the residual ratio of Mg is equal to that of the adsorbent,  $\gamma$  can be expressed by the following equation:

$$\gamma = W_{\text{Mgf}}/W_{\text{Mg}0} \times 100. \quad (13)$$

The concentration of the adsorbent remaining in the solid phase 24 h after adding the adsorbent,  $W_{\text{Adf}}/V$  [g/L], is as follows:

$$W_{\text{Adf}}/V = (\gamma/100) W_{\text{Ad}0}/V. \quad (14)$$

Therefore,  $Q_{\text{AS}}$  and the  $Q_F$  can be determined using the following equations:

$$Q_{\text{AS}} = (C_{\text{AS}0} - C_{\text{AS}})/(W_{\text{Adf}}/V). \quad (15)$$

$$Q_F = (C_{\text{F}0} - C_{\text{F}})/(W_{\text{Adf}}/V). \quad (16)$$

where the units for both  $Q_{\text{AS}}$  and  $Q_F$  are mg/g.

#### 4.5. Langmuir Isotherm Model

The suitability of the Langmuir isotherm model, which is a common adsorption model, was verified using the adsorption data obtained from the As–F simultaneous removal tests.

Langmuir isotherm plots for As-adsorption are shown in Figure 11. Figure 11a–c show  $\text{MgO}$ ,  $\text{Mg(OH)}_2$ , and  $\text{MgCO}_3$ , respectively.

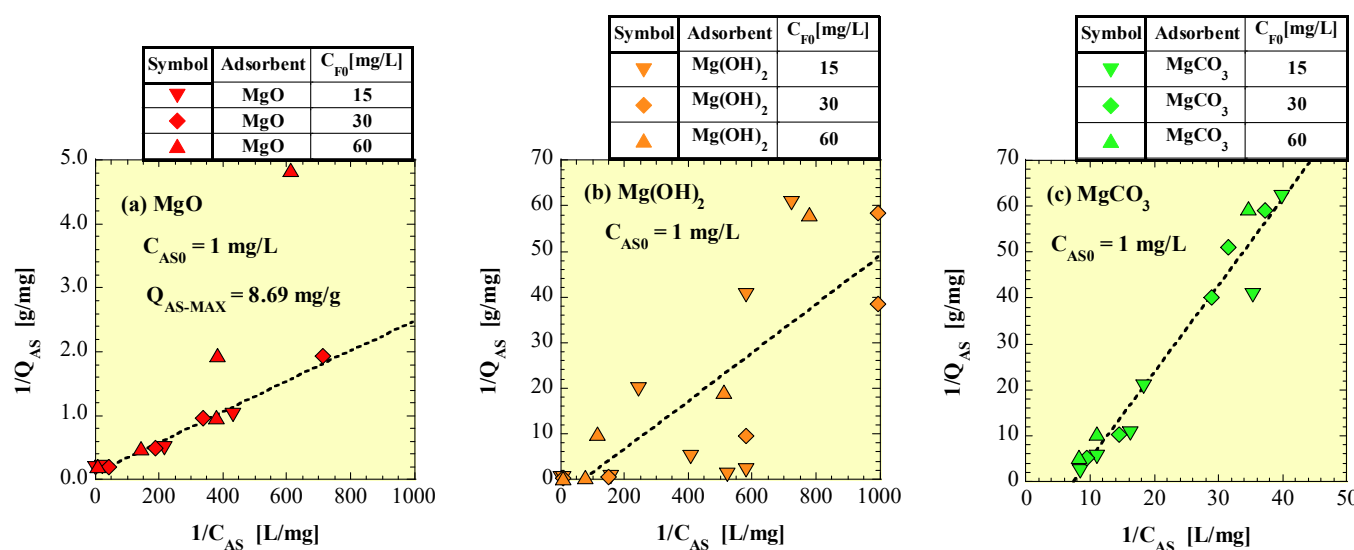


**Figure 11.** Langmuir isotherm plots for As(V): (a) MgO, (b) Mg(OH)<sub>2</sub>, and (c) MgCO<sub>3</sub>.

The Langmuir equation for As-adsorption is described by Equation (17):

$$1/Q_{AS} = 1/(K_L Q_{AS-MAX})(1/C_{AS}) + 1/Q_{AS-MAX}. \quad (17)$$

where  $Q_{AS-MAX}$  is the maximum As-adsorption amount [mg/g], and  $K_L$  is the Langmuir adsorption constant.

The As-adsorption data for MgO were plotted on a straight line, except for the upper two points in Figure 11a. An approximately straight line was obtained based on all the adsorption data for Mg(OH)<sub>2</sub>, as shown in Figure 11b, and the plots diverged significantly from the straight line. An approximately straight line was obtained based on all the adsorption data for MgCO<sub>3</sub>, as shown in Figure 11c, and the plots were almost straight. The intercept of the approximately straight line in Figure 11a yielded a  $Q_{AS-MAX}$  of 8.69 mg/g. The intercepts of the approximately straight lines for Mg(OH)<sub>2</sub> and MgCO<sub>3</sub> were negative. Therefore, the adsorption data for As based on these two Mg-based adsorbents did not fit the Langmuir isotherm model. For reference, the values of  $Q_{AS-MAX}$ ,  $K_L$ , and correlation coefficient  $r$  for the approximate straight lines obtained by applying Equation (17) to the As-adsorption data are listed in Table 2.

**Table 2.** Values of  $Q_{AS-MAX}$ ,  $K_L$ , and  $r$  for the approximate straight lines obtained by applying Equation (17) to As-adsorption data.

Figure No.	Adsorbent	$Q_{AS-MAX}$ (mg/g)	$K_L$	$r$
Figure 11a	MgO	8.69 *	48.7 *	0.988 *
Figure 11b	Mg(OH) <sub>2</sub>	-0.284 **	-66.9 **	0.791
Figure 11c	MgCO <sub>3</sub>	-14.0 **	-7.40 **	0.976

\* These values were calculated after excluding two adsorption data points that deviated significantly. \*\* The values are for reference only, as they did not fit the Langmuir model.

The Langmuir isotherm plots for the adsorption of F are shown in Figure 12. Figure 12a–c show MgO, Mg(OH)<sub>2</sub>, and MgCO<sub>3</sub>, respectively.

The Langmuir equation for F-adsorption is given by Equation (18):

$$1/Q_F = (1/K_L Q_{F-MAX})(1/C_F) + 1/Q_{F-MAX}. \quad (18)$$

where  $Q_F$  is the F-adsorption amount per mass of adsorbent [mg/g], and  $Q_{F-MAX}$  is the maximum F-adsorption amount [mg/g].

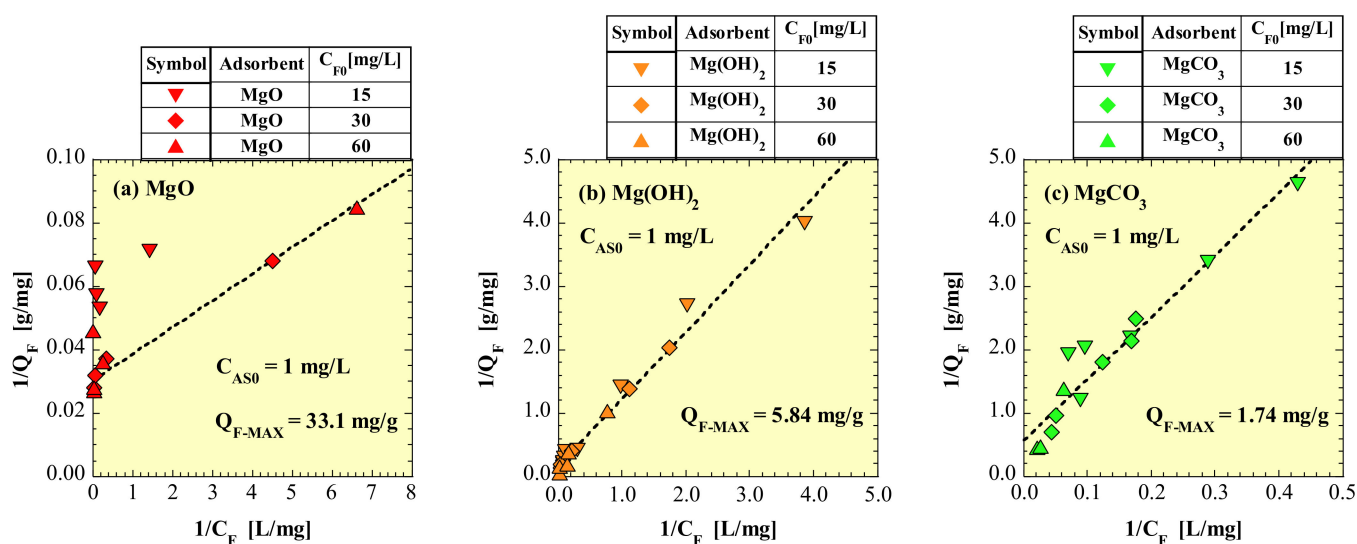


**Figure 12.** Langmuir isotherm plots for F: (a) MgO, (b) Mg(OH)<sub>2</sub>, and (c) MgCO<sub>3</sub>.

In Figure 12a, the plots of F-adsorption data for MgO are scattered. Therefore, an approximately straight line for MgO was obtained by excluding all data at  $C_{F0} = 15 \text{ mg/L}$  and one data point at  $C_{F0} = 60 \text{ mg/L}$ . The intercept of the approximately straight line in Figure 12a yields a  $Q_{F-MAX}$  of  $33.1 \text{ mg/g}$ . In contrast, the F-adsorption data for Mg(OH)<sub>2</sub> and MgCO<sub>3</sub> are plotted around approximately straight lines (Figure 12b,c). The intercepts of the approximately straight lines in Figure 12b,c give a  $Q_{F-MAX}$  of  $5.84 \text{ mg/g}$  for Mg(OH)<sub>2</sub> and  $1.74 \text{ mg/g}$  for MgCO<sub>3</sub>, respectively. For reference, the values of  $Q_{F-MAX}$ ,  $K_L$ , and  $r$  for the approximately straight lines obtained by applying Equation (18) for the F-adsorption data are listed in Table 3. The suitability of the F-adsorption data for Mg-based adsorbents in the Langmuir isotherm model was determined to be good for both Mg(OH)<sub>2</sub> and MgCO<sub>3</sub> but not for MgO. The  $pH_f$  range obtained in this test was 10.8–11.3 for the MgO tests, 10.2–10.6 for the Mg(OH)<sub>2</sub> tests, and 10.3–10.5 for the MgCO<sub>3</sub> tests (Figure 3). Most of the  $pH_f$  values in the MgO tests with  $C_{F0} = 15 \text{ mg/L}$  were less than 10.9. Thus, it can be inferred that the F-adsorption behavior of Mg-based adsorbents differed above and below approximately 10.9 of  $pH_f$ .

**Table 3.** Values of  $Q_{F-MAX}$ ,  $K_L$ , and  $r$  for the approximate straight lines obtained by applying Equation (18) to F-adsorption data.

Figure No.	Adsorbent	$Q_{F-MAX}$ (mg/g)	$K_L$	$r$
Figure 12a	MgO	33.1 *	3.62 *	0.991 *
Figure 12b	Mg(OH) <sub>2</sub>	5.84	0.161	0.991
Figure 12c	MgCO <sub>3</sub>	1.74	0.0586	0.964

\* These values were calculated by excluding all data at  $C_{F0} = 15 \text{ mg/L}$  and one data point at  $C_{F0} = 60 \text{ mg/L}$ , which deviated significantly.

#### 4.6. Freundlich Isotherm Model

Similar to the Langmuir isotherm model, the suitability of the Langmuir isotherm model was verified using adsorption data obtained from the As-F simultaneous removal tests.

The Freundlich isotherm plots for As-adsorption are shown in Figure 13. Figure 13a–c show MgO, Mg(OH)<sub>2</sub>, and MgCO<sub>3</sub>, respectively.

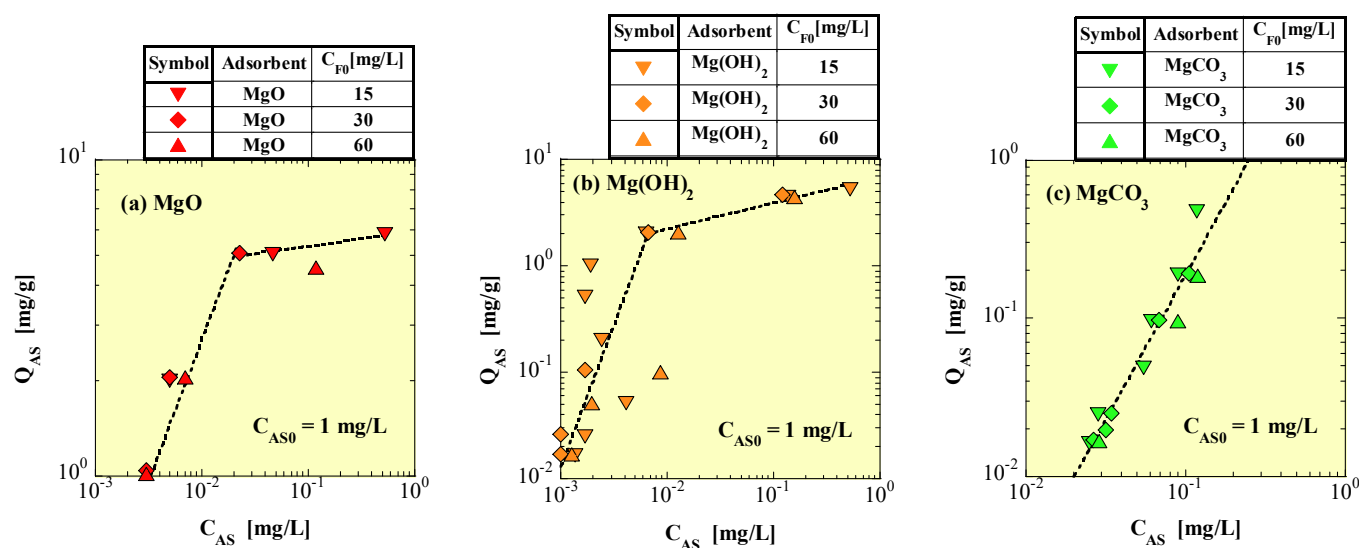


**Figure 13.** Freundlich isotherm plots for As(V): (a) MgO, (b) Mg(OH)<sub>2</sub>, and (c) MgCO<sub>3</sub>.

The Freundlich equation for As-adsorption is given by Equation (19):

$$Q_{AS} = K_F C_{AS}^{(1/n)}. \quad (19)$$

where  $K_F$  and  $n$  are Freundlich adsorption constants.

The approximate curves for MgO and Mg(OH)<sub>2</sub> are shown as two curves with different slopes, respectively. This is because, in the Freundlich plots,  $Q_{AS}$  approaches the saturation value with increasing  $C_{AS}$  and then  $Q_{AS}$  levels when  $C_{AS}$  exceeds a certain value. Therefore, the suitability of the Freundlich model is evaluated within a range lower than  $C_{AS}$ , where the slope of the approximate curve decreases.

The As-adsorption data for MgCO<sub>3</sub> fit the Freundlich isotherm model. In addition, the As-adsorption data for MgO in the low  $C_{AS}$  concentration range fit the Freundlich isotherm model. However, the adsorption data plots for Mg(OH)<sub>2</sub> are scattered and poorly fit the Freundlich isotherm model. For reference, the approximately straight line obtained by excluding some significantly deviating adsorption data is shown in Figure 13b. In addition, the values of  $K_F$ ,  $n$ , and  $r$  for the approximately straight lines obtained by applying Equation (19) to the As-adsorption data are listed in Table 4.

**Table 4.** Values of  $K_F$ ,  $n$ , and  $r$  for the approximately straight lines obtained by applying Equation (19) to As-adsorption data.

Figure No.	Adsorbent	$K_F$	$n$	$r$
Figure 13a	MgO	162	1.12	0.965
Figure 13b	Mg(OH) <sub>2</sub>	6.86 *	4.10 *	0.964 *
Figure 13c	MgCO <sub>3</sub>	12.6	0.547	0.856

\* These values were calculated by excluding significantly deviating As-adsorption data.

Subsequently, the Freundlich isotherm plots for F-adsorption are shown in Figure 14. Figure 14a–c show MgO, Mg(OH)<sub>2</sub>, and MgCO<sub>3</sub>, respectively.

The Freundlich equation for F-adsorption is given by Equation (20):

$$Q_F = K_F C_F^{(1/n)} \quad (20)$$

The values of  $K_F$ ,  $n$ , and  $r$  for approximately straight lines obtained by applying Equation (20) to the F-adsorption data are listed in Table 5.

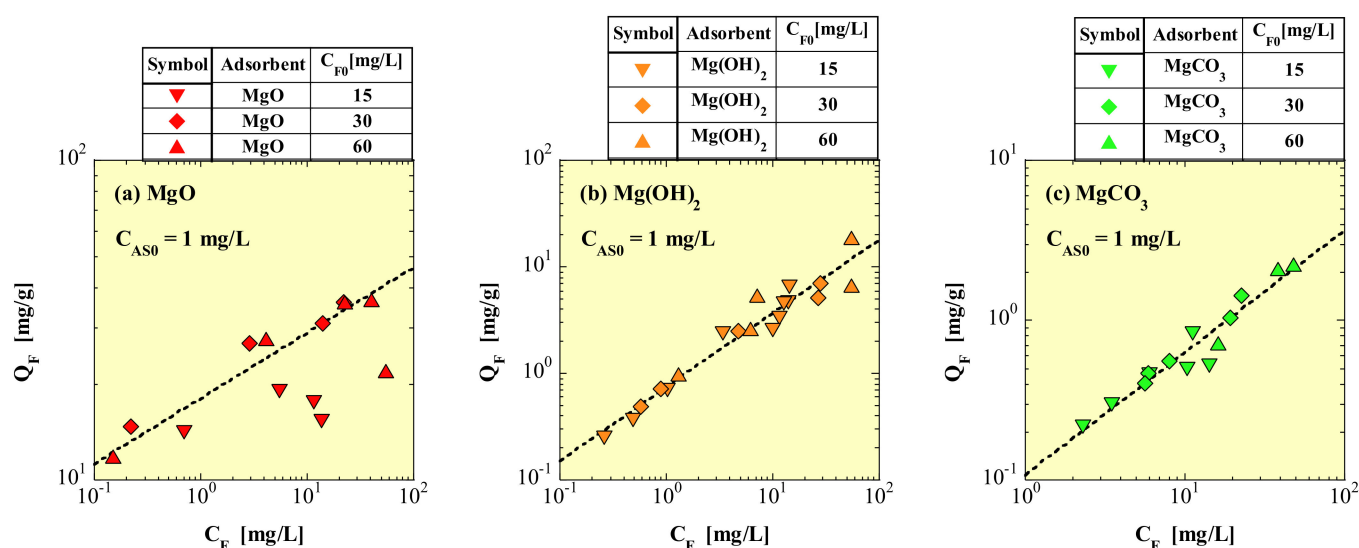


**Figure 14.** Freundlich isotherm plots for F: (a) MgO, (b) Mg(OH)<sub>2</sub>, and (c) MgCO<sub>3</sub>.

**Table 5.** Values of  $K_F$ ,  $n$ , and  $r$  for the approximately straight lines obtained by applying Equation (20) to F-adsorption data.

Figure No.	Adsorbent	$K_F$	$n$	$r$
Figure 14a	MgO	18.0 *	4.89 *	0.942 *
Figure 14b	Mg(OH) <sub>2</sub>	0.746	1.45	0.846
Figure 14c	MgCO <sub>3</sub>	0.108	1.31	0.973

\* These values were calculated by excluding significantly deviating F-adsorption data.

The F-adsorption data for Mg(OH)<sub>2</sub> and MgCO<sub>3</sub> fit the Freundlich isotherm model. Although several data points for MgO are plotted in the lower right of the approximation curve in Figure 14a, most of the adsorption data for MgO seem to fit the Freundlich isotherm model. The data plots that deviated from the approximate curve were the adsorption data with a  $pH_f$  of less than 10.9. Therefore, similar to the Langmuir model, the Freundlich model suggests that the F-adsorption behavior of Mg-based adsorbents differed above and below approximately 10.9 of  $pH_f$ .

Evaluation methods similar to this study were also used by Tolou et al. (2023), who studied the adsorption of As(III) and F on GO-MnO<sub>2</sub> [22]. They reported that the Langmuir isotherm model better fit the adsorption of As(III) in the presence of F-, and the Freundlich isotherm model better fit the adsorption of F- in the presence of As(III). The trend of suitability of As(V) and F for the MgCO<sub>3</sub> adsorbent in this study is similar to that of As(III) and F in the adsorption models for the GO-MnO<sub>2</sub>.

#### 4.7. Correlation of $pH_f$ with $C_{Mg}$ and $ORP_f$

To confirm whether there was a correlation between  $C_{Mg}$  and  $ORP_f$  with  $pH_f$ ,  $C_{Mg}$  and  $ORP_f$  were plotted versus  $pH_f$  in Figure 15a,b, respectively. Approximate curves obtained using the MgO data are shown in each figure.

As shown in Figure 15a, a negative correlation was found between  $pH_f$  and the logarithm of  $C_{Mg}$  for MgO, and the data for MgCO<sub>3</sub> were roughly plotted on the extension of the approximately straight line for MgO. The data for Mg(OH)<sub>2</sub> were plotted at positions that deviated significantly from the approximate curve for MgO, and no clear relationship was found between  $pH_f$  and  $C_{Mg}$  for Mg(OH)<sub>2</sub>.

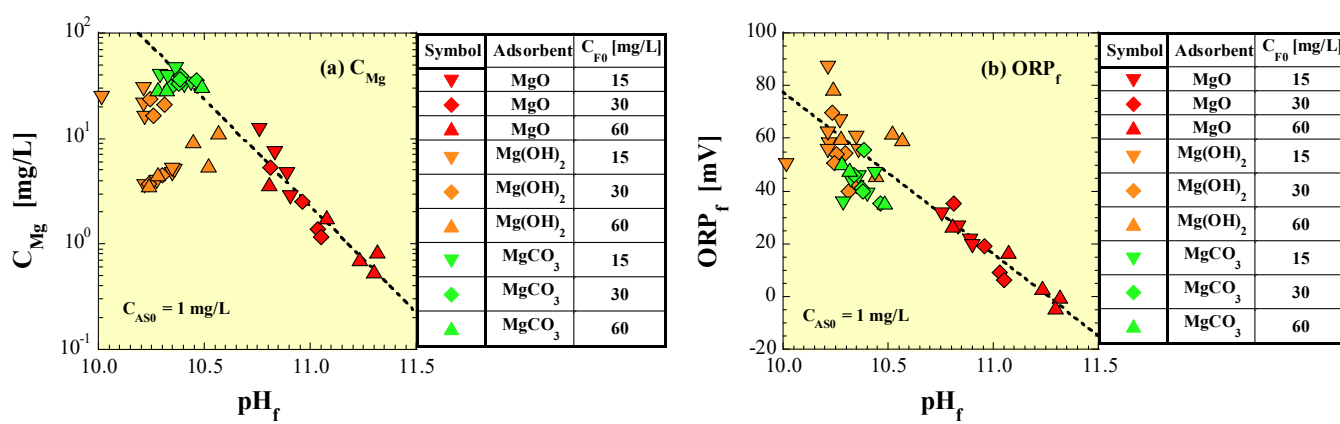


**Figure 15.** Plots of  $C_{Mg}$  and  $ORP_f$  versus  $pH_f$ : (a)  $C_{Mg}$  and (b)  $ORP_f$ .

In Figure 15b, a negative correlation was also found between  $pH_f$  and the  $ORP_f$  for MgO, and the data for  $Mg(OH)_2$  and  $MgCO_3$  appear to be plotted relatively close to the extension of the approximate straight line for MgO.

Furthermore, to consider the dissolution of the base materials of the adsorbents, after the conversion of the  $C_{Mg}$  and hydroxide ion concentration (calculated based on  $pH_f$ ) in the treatment of water-to-molar concentrations, the amount of  $\text{OH}^-$  in the solution was plotted versus the amount of Mg leached from the adsorbent as shown in Figure 16.  $M_{Mg}$  and  $[\text{OH}^-]_f$  are the molar concentrations of Mg [mM] and  $\text{OH}^-$  [mM], respectively, as shown in Figure 16.

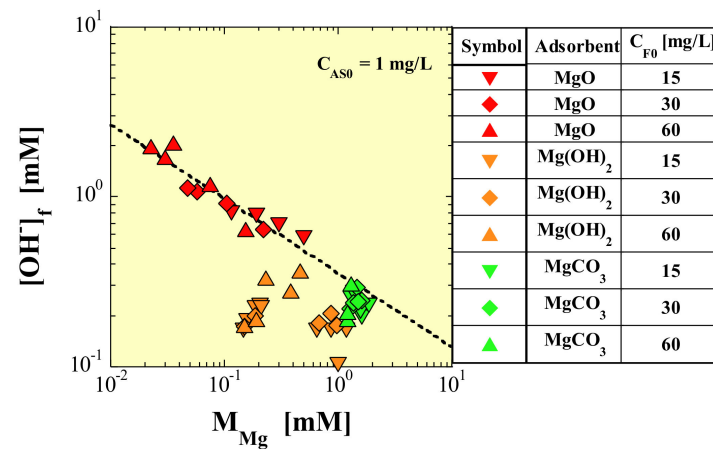
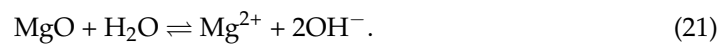


**Figure 16.** Plots of  $[\text{OH}^-]_f$  versus  $M_{Mg}$ .

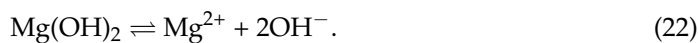
In Figure 16, a negative correlation was found between the  $M_{Mg}$  and the logarithm of  $[\text{OH}^-]_f$  for MgO, and the plots for  $Mg(OH)_2$  and  $MgCO_3$  are placed below the approximate straight line for MgO.

In this study, the dissolution reactions of the Mg-based adsorbent in water can be described as follows:

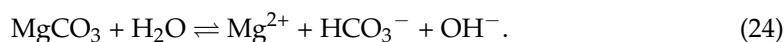
For the MgO-adsorbent,



For the  $Mg(OH)_2$ -adsorbent,



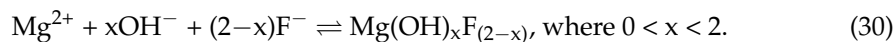
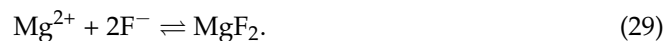
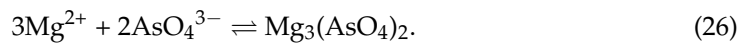
For the  $\text{MgCO}_3$ -adsorbent,



According to the above formulas, if  $M_{\text{Mg}}$  increases with the dissolution of the base materials of the Mg-based adsorbents,  $[\text{OH}^-]_f$  should also increase, though this did not actually occur. Therefore, the reaction mechanisms that differ from those in the above equation must be considered.

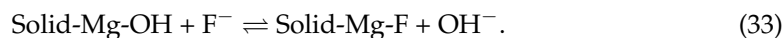
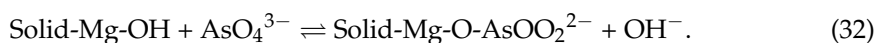
#### 4.8. Removal Mechanisms of As(V) and F

Based on the XRD results, the following precipitation reactions between  $\text{Mg}^{2+}$  leached from the Mg-based adsorbents and the arsenate ion species or  $\text{F}^-$  hardly occurred.



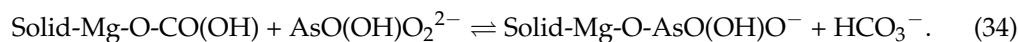
Nevertheless, As(V) and F were removed from the contaminated water, and it was presumed that ion-exchange chemical adsorption occurred on the surface of the Mg-based adsorbents, as shown in the following reaction equations:

Examples of the surface reaction of  $\text{MgO}$ - and  $\text{Mg(OH)}_2$ -adsorbents:



Considering the dissolved form of As(V) in the treated water estimated in Section 4.3, they considered that the reaction of Equation (31) was dominant for  $\text{Mg(OH)}_2$ , but for  $\text{MgO}$ , the reaction of Equation (32) also occurred with a comparable to higher frequency than that of Equation (31).

Examples of surface reaction of the  $\text{MgCO}_3$ -adsorbent:



Equations (31)–(33) denote the ion-exchange reactions with hydroxyl groups on the adsorbent surface, and Equations (34) and (35) denote the ion-exchange reactions with carbonate groups on the adsorbent surface. Monolayer adsorption reactions are generally believed to fit the Langmuir isotherm model. Because the adsorption data for F obtained in this study fit the Langmuir adsorption isotherms overall (Figure 12), the main F-removal mechanism by the Mg-based adsorbents was considered to be ion-exchange chemical adsorption on the adsorbent surface, as shown in Equations (33) and (35), respectively. However, the adsorption data of As(V) fit the Langmuir isotherm model only for  $\text{MgO}$

and not for  $\text{Mg}(\text{OH})_2$  or  $\text{MgCO}_3$ . Therefore, the As(V) removal mechanisms of Mg-based adsorbents cannot be explained by simple reactions, such as Equations (31) and (34), respectively. The results may indicate the influence of competitive adsorption between As(V) and F. However, the results of this study strongly support the conventional and general argument that arsenate ion species and  $\text{F}^-$  undergo ion-exchange with hydroxyl groups and carbonates on the adsorbent surface and are adsorbed. In addition, the removal performance of  $\text{MgCO}_3$  for As(V) and F is also supported as lower than that of  $\text{MgO}$  and  $\text{Mg}(\text{OH})_2$  because carbonate ion species, compared to hydroxide ions, have stronger competition for adsorption with arsenate ion species and  $\text{F}^-$ .

## 5. Conclusions

In this study, experiments were conducted to simultaneously remove As(V) and F from multiple contaminated water samples using Mg-based adsorbents. The effects of F on As(V) removal and the adsorption behavior of As(V) and F on the Mg-based adsorbents were examined. The removal performance of both As(V) and F followed the order  $\text{MgCO}_3 < \text{Mg}(\text{OH})_2 < \text{MgO}$ . For all three types of Mg-based adsorbents, regardless of  $C_{\text{F}0}$ , a considerable amount of F remained even when the majority of As(V) was removed. Thus, As(V) was preferentially adsorbed and removed by Mg-based adsorbents as opposed to F. Additionally, no magnesium arsenate, magnesium fluoride, or magnesium hydroxide fluoride species were observed in the XRD analysis. The adsorption data for F on Mg-based adsorbents generally fit the Langmuir and Freundlich isotherm models, with the exception of some data. The maximum F-adsorption amount  $Q_{\text{F-MAX}}$  obtained using the Langmuir model was 33.1, 5.84, and 1.74 mg/g for  $\text{MgO}$ ,  $\text{Mg}(\text{OH})_2$ , and  $\text{MgCO}_3$ , respectively, while the adsorption data of As(V) fit the Langmuir isotherm model only for  $\text{MgO}$ , and not for  $\text{Mg}(\text{OH})_2$  or  $\text{MgCO}_3$ . The maximum As-adsorption amount  $Q_{\text{AS-MAX}}$  obtained using the Langmuir model was 8.69 mg/g for  $\text{MgO}$ . In addition, the As(V) adsorption data fit the Freundlich isotherm model for  $\text{MgO}$  and  $\text{MgCO}_3$  but not for  $\text{Mg}(\text{OH})_2$ . Because magnesium arsenate,  $\text{MgF}_2$ , and magnesium hydroxide fluoride species were not observed in the XRD analysis, the removal mechanisms of As(V) and F by the Mg-based adsorbents were predominantly ion-exchange chemical-adsorption reactions with the hydroxyl or carbonate groups on the adsorbent surface. In the near future, we plan to conduct chemical equilibrium calculations based on the measurements of the Mg concentration, pH, and ORP obtained in this study and to further investigate the dissolved forms and precipitates. This research aims to advance sustainable As treatment methods using inexpensive Mg-based adsorbents.

**Author Contributions:** Conceptualization, H.S.; methodology, H.S., T.S. and J.H.; formal analysis, H.S. and K.M.; investigation, H.S. and K.M.; resources, H.S., K.M. and J.H.; data curation, H.S. and K.M.; writing—original draft preparation, H.S. and K.M.; writing—review and editing, H.S., K.M., T.S. and J.H.; supervision, J.H.; project administration, H.S.; funding acquisition, J.H., T.S. and H.S. All authors have read and agreed to the published version of the manuscript.

**Funding:** This study received no external funding.

**Institutional Review Board Statement:** Not applicable.

**Informed Consent Statement:** Not applicable.

**Data Availability Statement:** Data supporting the findings of this study are available from the corresponding authors upon reasonable request.

**Acknowledgments:** We are deeply grateful to Terumi Oguma for her assistance with the experiments.

**Conflicts of Interest:** The authors declare no conflicts of interest.

## References

- Zhu, C.; Bai, G.; Liu, X.; Li, Y. Screening high-fluoride and high-arsenic drinking waters and surveying endemic fluorosis and arsenism in Shaanxi province in western China. *Water Res.* **2006**, *40*, 3015–3022. [CrossRef] [PubMed]
- Armienta, M.A.; Segovia, N. Arsenic and fluoride in the groundwater of Mexico. *Environ. Geochem. Health* **2008**, *30*, 345–353. [CrossRef] [PubMed]
- Farooqi, A.; Masuda, H.; Siddiqui, R.; Naseem, M. Sources of Arsenic and Fluoride in Highly Contaminated Soils Causing Groundwater Contamination in Punjab, Pakistan. *Arch. Environ. Contam. Toxicol.* **2009**, *56*, 693–706. [CrossRef] [PubMed]
- Ingallinella, A.M.; Pacini, V.A.; Fernandez, R.G.; Vidoni, R.M.; Sanguinetti, G. Simultaneous removal of arsenic and fluoride from groundwater by coagulation-adsorption with polyaluminum chloride. *J. Environ. Sci. Health A* **2011**, *46*, 1288–1296. [CrossRef] [PubMed]
- Alarcon-Herrera, M.T.; Bundschuh, J.; Nath, B.; Nicollid, H.B.; Gutierrez, M.; Reyes-Gomez, V.M.; Nunez, D.; Martín-Dominguez, I.R.; Sracek, O. Co-occurrence of arsenic and fluoride in groundwater of semi-arid regions in Latin America: Genesis, mobility and remediation. *J. Hazard. Mater.* **2013**, *262*, 960–969. [CrossRef] [PubMed]
- Navarro, O.; González, J.; Júnez-Ferreira, H.E.; Bautista, C.-F.; Cardona, A. Correlation of Arsenic and Fluoride in the groundwater for human consumption in a semiarid region of Mexico. *Procedia Eng.* **2017**, *186*, 333–340. [CrossRef]
- Jha, P.K.; Tripathi, P. Arsenic and fluoride contamination in groundwater: A review of global scenarios with special reference to India. *Groundw. Sustain. Dev.* **2021**, *13*, 10057. [CrossRef]
- The World Health Organization (WHO). *Guidelines for Drinking-Water Quality*, 4th ed.; Arsenic, 315–318; WHO: Tarxien, Malta, 2011; ISBN 978-92-4-154815-1. Available online: [https://apps.who.int/iris/bitstream/handle/10665/44584/9789241548151\\_eng.pdf](https://apps.who.int/iris/bitstream/handle/10665/44584/9789241548151_eng.pdf) (accessed on 10 December 2023).
- Jadhav, S.V.; Bringas, E.; Yadav, G.D.; Rathod, V.K.; Ortiz, I.; Marathe, K.V. Arsenic and fluoride contaminated groundwaters: A review of current technologies for contaminants removal. *J. Environ. Manag.* **2015**, *162*, 306–325. [CrossRef]
- Sarkar, A.; Paul, B. The global menace of arsenic and its conventional remediation—A critical review. *Chemosphere* **2016**, *158*, 37–49. [CrossRef]
- Ghosh, S.; Debsarkar, A.; Dutta, A. Technology alter-natives for decontamination of arsenic-rich groundwater—A critical review. *Environ. Technol. Innov.* **2019**, *13*, 277–303. [CrossRef]
- Kumar, R.; Patel, M.; Singh, P.; Bundschuh, J.; Pittman, C.U., Jr.; Trakal, L.; Mohan, D. Emerging technologies for arsenic removal from drinking water in rural and peri-urban areas: Methods, experience from, and options for Latin America. *Sci. Total Environ.* **2019**, *694*, 133427. [CrossRef]
- Yu, X.Y.; Luo, T.; Jia, Y.; Zhang, Y.X.; Liu, J.H.; Huang, X.J. Porous hierarchically micro-/nanostructured MgO: Morphology control and their excellent performance in As(III) and As(V) removal. *J. Phys. Chem. C* **2011**, *115*, 22242–22250. [CrossRef]
- Lin, Q.; Chen, W.; Lin, F.; Zhu, H.; Wang, X. Exaggerated arsenic removal efficiency and pH adaptability by adsorption using monodispersed porous pinecone-like magnesium hydroxide. *AQUA* **2023**, *72*, 969–982. [CrossRef]
- Mohapatra, M.; Anand, S.; Mishra, B.K.; Giles, D.E.; Singh, P. Review of fluoride removal from drinking water. *J. Environ. Manag.* **2009**, *91*, 67–77. [CrossRef]
- He, J.; Yang, Y.; Wu, Z.; Xie, C.; Zhang, K.; Kong, L.; Liu, J. Review of fluoride removal from water environment by adsorption. *J. Environ. Chem. Eng.* **2020**, *8*, 104516. [CrossRef]
- Gai, W.-Z.; Deng, Z.-Y. A comprehensive review of adsorbents for fluoride removal from water: Performance, water quality assessment and mechanism. *Environ. Sci. Water Res. Technol.* **2021**, *7*, 1362–1386. [CrossRef]
- Pillai, P.; Dharaskar, S.; Pandian, S.; Panchal, H. Overview of fluoride removal from water using separation techniques. *Environ. Technol. Innov.* **2021**, *21*, 101246. [CrossRef]
- Jin, Z.; Jia, Y.; Zhang, K.-S.; Kong, L.-T.; Sun, B.; Shen, W.; Meng, F.-L.; Liu, J.-H. Effective removal of fluoride by porous MgO nanoplates and its adsorption mechanism. *Appl. Surf. Sci.* **2015**, *357*, 1080–1088. [CrossRef]
- Wallace, A.R.; Su, C.; Sun, W. Adsorptive removal of fluoride from water using nanomaterials of ferrihydrite, apatite, and brucite: Batch and column studies. *Environ. Eng. Sci.* **2019**, *36*, 634–642. [CrossRef]
- Lopez-Guzman, M.; Alarcon-Herrera, M.T.; Irigoyen-Campuzano, J.R.; Torres-Castanon, L.A.; Reynoso-Cuevas, L. Simultaneous removal of fluoride and arsenic from well water by electrocoagulation. *Sci. Total Environ.* **2019**, *678*, 181–187. [CrossRef]
- Tolkou, A.K.; Trikkaliotis, D.G.; Kyzas, G.Z.; Katsoyiannis, I.A.; Deliyanni, E.A. Simultaneous Removal of As(III) and Fluoride Ions from Water Using Manganese Oxide Supported on Graphene Nanostructures (GO-MnO<sub>2</sub>). *Sustainability* **2023**, *15*, 1179. [CrossRef]
- Sugita, H.; Oguma, T.; Zhang, M.; Hara, J.; Takahashi, S. Environmental stability of spent magnesium-based and calcium-based arsenic adsorbents-Effects of soils. *J. Jpn. Soc. Civ. Eng. Ser. G Environ. Res.* **2016**, *72*, 437–448. [CrossRef]
- Rojo, J.M.; Mesa, J.L.; Pizarro, J.L.; Lezama, L.; Arriortua, M.I.; Rojo, T. Spectroscopic and Magnetic Study of the (Mg,M)<sub>3</sub>(AsO<sub>4</sub>)<sub>2</sub>·8H<sub>2</sub>O (M = Ni<sup>2+</sup>, Co<sup>2+</sup>) Arsenates. *Mater. Res. Bull.* **1996**, *31*, 925–934. [CrossRef]
- Ferraris, G.; Franchini-Angela, M. Hydrogen Bonding in the Crystalline State. Crystal Structure of MgHAsO<sub>4</sub>·7H<sub>2</sub>O, Roesslerite. *Acta. Crystallogr. B* **1973**, *29*, 286–292. [CrossRef]
- Baur, W.H.; Khan, A.A. Rutile-type Compounds. IV. SiO<sub>2</sub>, GeO<sub>2</sub> and a Comparison with Other Rutile-type Structures. *Acta Crystallogr. B* **1971**, *27*, 2133–2139. [CrossRef]

27. Crichton, W.A.; Parise, J.B.; Muller, H.; Breger, J.; Marshall, W.G.; Welch, M.D. Synthesis and Structure of Magnesium Hydroxide Fluoride, Mg(OH)F: A Topological Intermediate Between Brucite- and Rutile-type Structures. *Mineral. Mag.* **2012**, *76*, 25–36. [[CrossRef](#)]
28. The Chemical Society of Japan (CSJ). *Kagaku Binran (Handbook of Chemistry), Pure Chemistry II*, 5th ed.; Maruzen: Tokyo, Japan, 2004; p. 332.

**Disclaimer/Publisher’s Note:** The statements, opinions and data contained in all publications are solely those of the individual author(s) and contributor(s) and not of MDPI and/or the editor(s). MDPI and/or the editor(s) disclaim responsibility for any injury to people or property resulting from any ideas, methods, instructions or products referred to in the content.